CRYSTAL GROWTH & DESIGN

Article

pubs.acs.org/crystal

Adipic Acid Primary Nucleation Kinetics from Probability Distributions in Droplet-Based Systems under Stagnant and Flow Conditions

Damiano Rossi,[†] Asterios Gavriilidis,[†] Simon Kuhn,[‡] Miguel Ardid Candel,[†] Alan G. Jones,[†] Chris Price,[§] and Luca Mazzei*,[†]

[†]University College London, Department of Chemical Engineering, Torrington Place, London WC1E 7JE, U.K.

[‡]KU Leuven, Department of Chemical Engineering, W. de Croylaan 46, 3001 Leuven, Belgium

[§]University of Strathclyde, Department of Chemical Engineering, 75 Montrose Street, Glasgow G1 1XJ, Scotland

Supporting Information

ABSTRACT: In this work, we present a microfluidic approach that allows performing nucleation studies under different fluid dynamic conditions. We determine primary nucleation rates and nucleation kinetic parameters for adipic acid solutions by using liquid/liquid segmented flow in capillary tubes in which the crystallizing medium is partitioned into small droplets. We do so by measuring the probability of crystal presence within individual droplets under stagnant (motionless droplets) and flow (moving droplets) conditions as a function of time, droplet volume, and supersaturation. Comparing the results of the experiments with the predictions of the classical nucleation theory model and of the mononuclear nucleation mechanism model, we conclude that adipic acid nucleates mainly via a heterogeneous mechanism under both fluid dynamic conditions. Furthermore, we show that the flow conditions enhance the primary nucleation rate by increasing the kinetic parameters of the process without affecting the thermodynamic parameters. In this regard, a possible mechanism is discussed on the basis of the enhancement of the attachment frequency of nucleation caused by the internal recirculation that occurs within moving droplets.

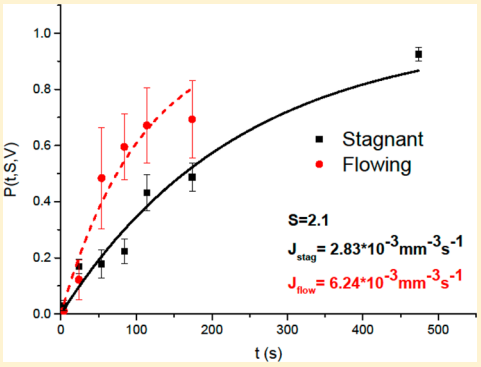

1. INTRODUCTION

Cooling crystallization from supersaturated solution is the crystallization method most frequently employed in the pharmaceutical industry. Nucleation represents the first step of the entire crystallization process, in which molecules arrange themselves in patterns characteristic of a crystalline solid, forming sites wherein additional particles attach and grow into crystals. It is well established that nucleation is a stochastic phenomenon, so that predicting deterministically where nucleation events will take place within a given volume is impossible.[1] For this reason, we may adopt two strategies to determine nucleation kinetics. We can work with a single, large volume, which owing to its size behaves deterministically, or with a large number of small, noninteracting volumes, which owing to their size behave stochastically. In the first case, at least in theory, one experiment suffices for deriving nucleation rates,[2] while in the second case, to obtain the kinetics, one needs to consider the results of a large set of statistically independent, small-volume experiments.[3] In spite of the advantages that the deterministic approach offers in terms of (simple) experimental setup, this method makes it hard to operate isothermally under uniform fluid dynamic conditions (owing to the large dimensions of the setup), rendering the system difficult to operate, control, and analyze.

Microfluidics offers great potential for controlling and studying nucleation.[4] With the aim of generation of kinetic data, microfluidic devices are useful tools for screening crystallization, for they offer good control of transport phenomena (enhanced mass and heat transfer), little gravity effect, and few impurities.[5] Moreover, in specific channel geometries, two-phase flows can produce nearly monodisperse droplets.[6,7] The hundreds of droplets generated in the microfluidic chip yield a large set of independent nucleation events suitable for conducting a statistical analysis. For example, such systems have been used to calculate nucleation and growth rates for proteins by means of microliter droplets and "double-step" temperature profiles, respectively.[8] Droplet-based microfluidic crystallizers are also adopted for controlling crystal size by confining crystallization within nearly identical droplets that reside in the crystallizer for nearly equal times.[9] Various microfluidic devices and experimental procedures have been introduced in recent years to investigate crystal nucleation kinetics of several compounds in static arrays of monodisperse droplets.[10−14]

Received: December 18, 2014
Revised: February 24, 2015
Published: March 3, 2015

DOI: 10.1021/cg501836e
Cryst. Growth Des. 2015, 15, 1784−1791

In all the studies mentioned above, crystal nucleation occurs under quiescent conditions. In this work, conversely, we focus on primary nucleation within droplets under both stagnant (motionless droplets) and flow (moving droplets) conditions to study if and how the mixing, generated within the droplets by the flow, affects the nucleation kinetics. To this end, we employ a versatile and flexible capillary crystallizer with a T-shaped junction for droplet generation. We control nucleation residence times by varying the length of the capillary and supersaturation by varying the temperature of the mixture. The two-phase system also permits us to avoid clogging issues, to which small channels are prone.[15] We finally discuss the nucleation rates and kinetics determined experimentally by resorting to the classical nucleation theory (CNT) and the mononuclear nucleation mechanism (MNM) for both fluid dynamic conditions.

2. THEORY

Although the nucleation process is stochastic, the primary nucleation rate $J(S)$ can be regarded as a deterministic quantity. This is because $J(S)$, which represents the expected (or mean) number of nuclei generated per unit volume and time at a given supersaturation ratio S, refers to volumes that are sufficiently large to eliminate the stochastic (or random) nature of the process. For conventional batch crystallizers, one can thus adopt a deterministic modeling approach, on the basis of the population balance equation,[16] describing nucleation directly in terms of $J(S)$. On the other hand, for small-volume systems (droplets), one needs to resort to a statistical modeling approach.[14] The most reliable way of measuring crystal nucleation kinetics is the droplet method.[4] Each droplet behaves as a single (random) batch system, and a large number of such systems permits deriving the required statistics. In particular, one can obtain the cumulative distribution function $P(t;S,V)$, which represents the probability of detecting at least one crystal within a time t in a droplet of volume V (see Figure 1) at a given supersaturation ratio S.[17]

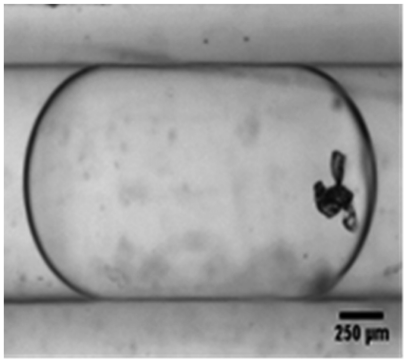

Figure 1. Adipic acid crystals in a water droplet.

The supersaturation ratio is defined as $S \equiv a/a_e$. Here a and a_e are respectively the actual and the equilibrium activities of a molecule in the solution. Because we work with dilute solutions, we assume that S reduces to C/C_e,[18] where C and C_e are the molar concentration of the solute and the solubility, respectively; the latter is a function of the solution temperature T.

If we denote as $M^+(t;S,V)$ the number of droplets in which at least a crystal forms within a time t and as M as the overall number of droplets considered, then

$$P_E(t;\ S,\ V) = M^+(t;\ S,\ V)/M \tag{1}$$

From a statistical standpoint, M needs to be large enough that its choice does not affect the value of $P_E(t;S,V)$. Equation 1 allows determining the cumulative distribution function experimentally.

When the droplet volume V is sufficiently small while the nucleation time t is large compared to the growth time, only mononuclear nucleation occurs.[19] In this case, since nucleation is a stochastic process, the probability $P(t;S,V)$ evolves as a stationary Poisson process.[14] Hence, the theoretical probability that at a given time t at least one crystal is present in a droplet of volume V containing a mixture at supersaturation S is equal to[11]

$$P_T(t;\ S,\ V) = 1 - \exp[-J(S)Vt] \tag{2}$$

Equation 2 permits determining the value of the nucleation rate J: that is, the number of nuclei formed per unit time and volume at a given supersaturation ratio S. Note that, even though eqs 1 and 2 involve the volume of the droplets as independent variable, the value of the nucleation rate does not depend on it; as reported in eq 2, J depends solely on the supersaturation ratio S. To obtain its value, we fit the theoretical function $P_T(t;S,V)$ with the experimental function $P_E(t;S,V)$. Note that the nucleation rate determined in this way refers to *primary nucleation*, inasmuch as the probability function $P(t;S,V)$ has to do only with the presence of (at least) one crystal: it is not concerned with the total number of crystals present in each droplet. Only the latter might be affected by the presence of secondary nucleation. The probability function relates only to primary nucleation.

In classical nucleation theory, the primary nucleation rate is given by[20]

$$J(S) = AS\ \exp[-B/(\ln S)^2] \tag{3}$$

where A and B are the kinetic and thermodynamic parameters for the selected compound. We may rewrite eq 3 equivalently as

$$y = \ln A - Bx \tag{4}$$

where

$$y \equiv \ln[J(S)/S] \text{ and } x \equiv 1/(\ln S)^2$$

If we repeat the experimental campaign described above for different values of S, we can obtain the function $y(x)$ and, from its linear diagram, the values of the parameters A and B (from the intercept and the slope of the line, respectively).

A and B are related to other variables of interest such as the nucleus size n^*, the nucleation work W, the Zeldovich factor z, the attachment frequency f^*, the concentration of nucleation sites C_0, and the crystal−liquid interfacial energies for homogeneous and heterogeneous nucleation, here denoted as γ and γ_{eff}, respectively.[18] These, except for γ, are all functions of A, B, and S; their expressions are given by the classical theory developed over many years by Gibbs, Volmer, Weber, Becker, Doring, Turnbull, and Fisher.[20] In particular

DOI: 10.1021/cg501836e
Cryst. Growth Des. 2015, 15, 1784−1791

$$n^* = \frac{2B}{(\ln S)^3} \quad W = \frac{KT \ln Sn^*}{2} \quad z = \left[\frac{W}{3\pi KT(n^*)^2}\right]^{1/2}$$
$$f^*C_0 = \frac{AS}{z} \quad \gamma_{\text{eff}} = \frac{KT}{c}\left[\frac{27B}{4v_0^2}\right]^{1/3} \tag{5}$$

Here K is the Boltzmann constant (1.381×10^{-20} mJ K^{-1}), T the solution temperature, v_0 the volume of a molecule of solute in the crystalline state (1.78×10^{-28} m^3 for adipic acid), and c the shape factor of the crystal (this is a dimensionless quantity that relates the surface area Σ of an object to its volume φ and is defined as $c = \Sigma/(\varphi^{2/3})^{20}$). Crystals are usually assumed to be spherical, so that c is taken to be $(36\pi)^{1/3}$.

So far, two approaches have been most widely used in the literature to determine the nucleation rate $J(S)$: the polynuclear nucleation mechanism (PNM) and mononuclear nucleation mechanism (MNM). The former assumes that, when nucleation starts taking place, several stable nuclei appear simultaneously in the solution; these are observed only when their size has increased sufficiently for detection. Conversely, the latter mechanism assumes that nucleation originates via a single crystal; once formed, this grows and subsequently, owing to abrasion, attrition, shearing action, or breakage, it fragments, generating (by secondary nucleation) many new nuclei which then grow into detectable crystals. The MNM and PNM approaches model different processes that are encountered in reality and lead to different expressions for the cumulative distribution function $P_T(t;S,V)$, because they describe two limiting cases of nucleation that can occur in practice. The MNM and PNM hold for small and large fluid volumes, respectively.[19] In this work, we determine the nucleation rate $J(S)$ using the mononuclear nucleation mechanism because the experimental conditions reflect the requirements for the applicability of such a model. The MNM has been used with promising results and good data fitting to describe nucleation in microfluidic devices; for instance, for m-ABA and L-His,[17,21] lysozyme,[22] and isonicotinamide,[3] assuming the MNM as the dominant nucleation mechanism, instead of the PNM, led to better experimental data fitting.

We conducted the nucleation study described above under stagnant conditions (motionless droplets) and flow conditions (moving droplets) with the experimental setup described in section 3.2. In segmented liquid−liquid (water/hexane) flow in small channels, as the liquid droplets move along the channel at constant speed, the fluid within them circulates, giving rise to counter-rotating vortices with closed streamlines and a pattern symmetrical about the channel axis.[23,24] This occurs because the dispersed phase (water) moves faster than the continuous phase (hexane), generating a slip between the two phases (refer to section 3). The mixing that takes place permits us to study the primary nucleation process under different fluid dynamic conditions, not only under stagnant conditions, which one normally encounters in nucleation studies where mass transfer is dominated by molecular diffusion.

3. EXPERIMENTAL SECTION

3.1. Chemicals. Adipic acid (hexanedioic acid, $(CH_2)_4(COOH)_2$, >99.5% pure, Sigma-Aldrich, U.K.) was used as received without further purification, and solutions were made in deionized water (conductivity <0.2 μS/cm). The solubility of adipic acid in water at various temperatures was determined from the solubility curve shown in Figure 2, which we derived by fitting experimental data reported in the literature.[25]

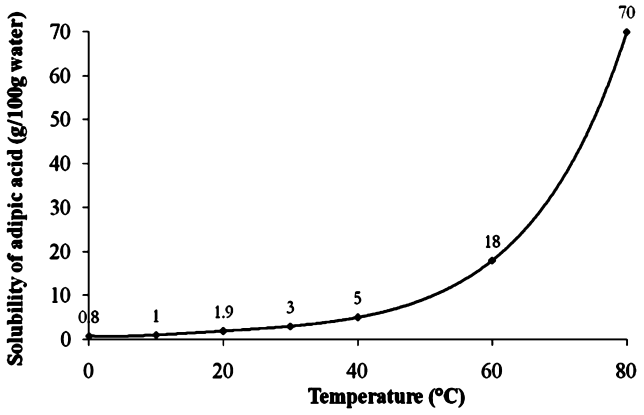

Figure 2. Solubility of adipic acid as a function of temperature.[25]

n-Hexane ($(CH_3)(CH_2)_4CH_3$ >97% pure, maximum 0.005% water, VHR, U.K.) was used as received, without further purification, and was the selected carrier fluid in the multiphase experiments.

3.2. Experimental Setup and Procedure. We studied nucleation by using liquid/liquid segmented flows in which the crystallizing aqueous solution is split into a series of droplets by hexane. Adipic acid solution droplets take on the characteristic capsular shape owing to the hydrophobicity of the internal capillary surface (Figure 3). Droplets can either completely or nearly completely fill the cross section of the channel. A thin liquid film of hexane separates them from the channel walls confining the nucleation process within the droplet volume, avoiding contact with the walls and thereby preventing clogging.

Figure 4 shows the schematic of the droplet-based capillary crystallizer setup adopted for stagnant and flow experiments. The two-phase flow is obtained with PFA capillaries (i.d. 1 mm, o.d. 1.5 mm) connected to two Harvard PHD 2000 syringe pumps followed by PCTFE (polychlorotrifluoroethene) filters (2 μm) and a PEEK T-junction (i.d. 0.5 mm). The pumps and T junction are located inside a Perspex enclosure in which the adipic acid solution is kept undersaturated at temperature T_1 = 30 °C.

Under stagnant conditions, droplet arrays were generated inside the enclosure at T_1 and manually moved to the nucleation section at T_2 (to reach the desired supersaturation S) and then to the growth section at T_3 to let crystals grow to reach an observable size, at a temperature very close to the saturation limit where no nucleation occurs. The temperature history is illustrated in Figure 5. In this way, nucleation times could be easily set. The nucleation and growth sections were two jacketed vessels connected to different water baths; this permitted setting the desired temperature. The growth time was kept constant, and 3 h was assumed to be sufficient for nuclei to reach a detectable size. The growth time does not affect the outcome of the experiments: the same values of the probability function $P_E(t;S,V)$ were found for growth times longer and shorter than 3 h. From a statistical standpoint a sufficiently large value of M was considered to be around 100[11]. For this reason, we decided to operate with arrays of 200 droplets (that is, M = 200 in eq 1).

We detected crystals by optical microscopy (Olympus IX50). To improve crystal detection and eliminate light reflection problems owing to the curvature of the capillary external surface, we used a refractive index matching device in the microscope unit. The capillary was immersed in a plastic box filled with water and fixed by guides that allowed moving the capillary and passing the droplets in front of the microscope lens.

The crystals present within each droplet after 3 h of growth were not clearly identifiable, as they tended to agglomerate (Figure 1). This occurred at all the supersaturations investigated. Adipic acid normally crystallizes from aqueous solutions as flat, slightly elongated, hexagonal, monoclinic plates. It is hard, however, to clearly identify this shape when crystals are not well isolated (Figure 1). We should also note that the light coming from the microscope had to pass through the refractive index matching device, the wall of the capillary,

DOI: 10.1021/cg501836e
Cryst. Growth Des. 2015, 15, 1784−1791

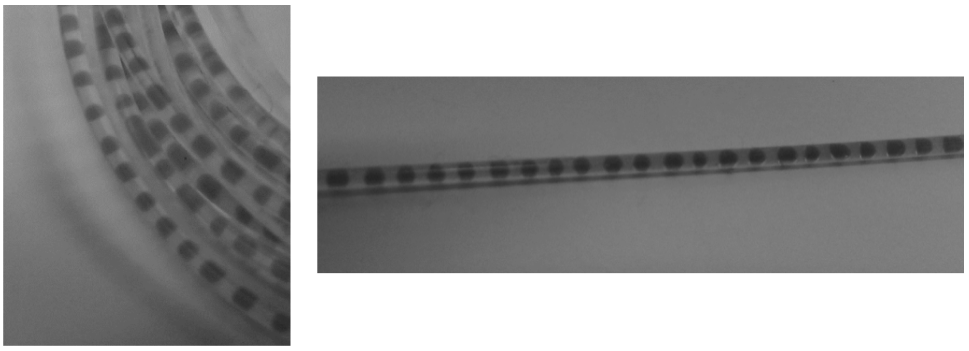

Figure 3. Basic blue 41 dye water solution/hexane droplet arrays in 1 mm PFA capillary tube.

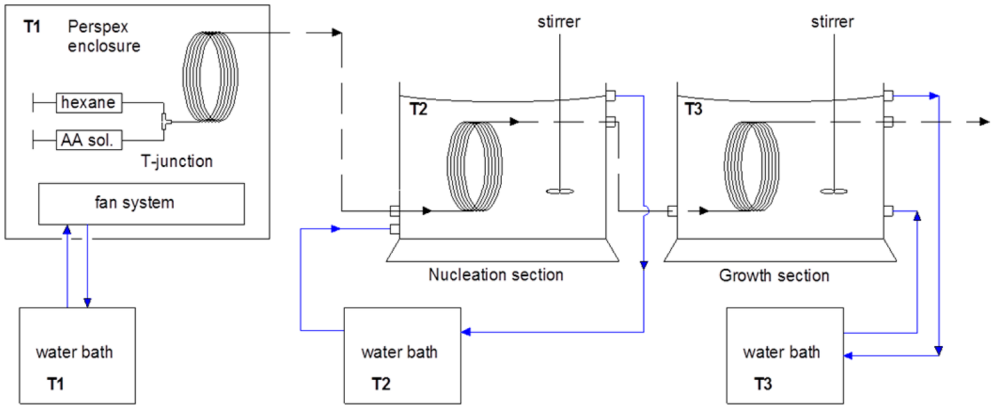

Figure 4. Droplet-based capillary crystallizer setup; dashed line for flow conditions.

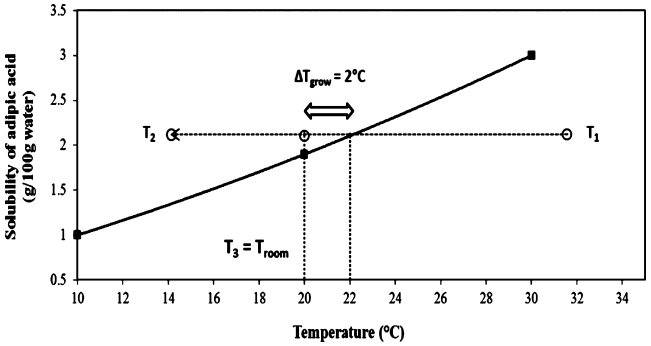

Figure 5. Temperature profile in droplet-based capillary crystallizer.

and the water droplet volume; this affected the quality of the images, introducing some shadows in the background. However, these detection issues did not pose problems in our investigation, as we only needed to know whether crystals were present or not in each droplet to obtain the cumulative probability function (eq 2). The crystal number and shape, as well as the structure of the agglomerates formed, were not critical aspects in our analysis.

As the laboratory room temperature was fixed at T_{room} = 20 °C, we chose the adipic acid solution concentration (2.1 g of adipic acid per 100 g of water; under this condition pH 3 was measured) so that the growth temperature T_3 coincided with the room temperature T_{room}. In this way, we did not have problems of crystal dissolution during the crystal detection process. T_3 was set to a temperature difference of ΔT_{growth} = 2 °C from the equilibrium solubility curve to make sure that no nucleation could occur in the growth section. We verified this experimentally by checking that, if we bypass the nucleation section, the value of the experimental cumulative probability function $P_E(t;S,V)$ after 3 h of growth at T_3 is 0.

We repeated under flow conditions the study performed under stagnant conditions, where we changed the residence time of the droplets in the channel by varying the length of the capillary immersed in the nucleation unit at the temperature T_2. To generate the droplets, we used the same water/hexane flow rates (0.3925 mL/min for both fluids) employed in the stagnant experiments. The droplets appeared to be stable with uniform total length L_d of ca. 2.2 mm and a corresponding constant volume of ca. V = 1.5 mm^3 (Figure 1). We estimated the latter by assuming that droplets have semispherical front and back sections. Once a water droplet forms, it is no longer in contact with the internal channel wall and a very thin film of liquid surrounds it. This film allows the droplet to travel at a relatively higher local velocity than the hexane slugs, and its thickness depends on the fluid system and the flow rates. We wrote an image processing program in Matlab to measure the water droplet and hexane slug volumes, obtained by recording pictures with a Fastcam MC1 Photron high-speed camera attached to the optical microscope. The presence of a slip velocity between the two phases is confirmed by the positive water/hexane slip velocity ratio (s = 1.15), which is calculated from the two-phase holdup.[26] This proves the presence of shear stress between the dispersed and continuous phases, which induces the internal recirculation within the droplets.

The values of the supersaturation ratio used are S = 2.1, 1.57, 1.39 and 1.23, obtained by cooling the droplet arrays to 10, 14, 16, and 18 °C, respectively. If adipic acid were significantly soluble in hexane, the values of the supersaturation ratio reported above could change owing to mass transfer of adipic acid from the drops to the slugs. To check whether adipic acid is soluble in hexane, we performed the following experiment. We added 5 g of adipic acid crystals to 100 mL of hexane in a glass beaker. We stirred the mixture for 24 h at 30 °C. Subsequently, we separated (by filtration) the undissolved adipic acid from the mother liquor and then we evaporated all the mother liquor. We repeated the same experiment at higher temperatures (35 and 40 °C), but we could never collect and weigh any crystals after evaporating the mother liquor. This proves that adipic acid is insoluble in hexane. As further evidence, no crystals have ever been detected in the hexane slugs after cooling under either stagnant or flow conditions.

DOI: 10.1021/cg501836e
Cryst. Growth Des. 2015, 15, 1784−1791

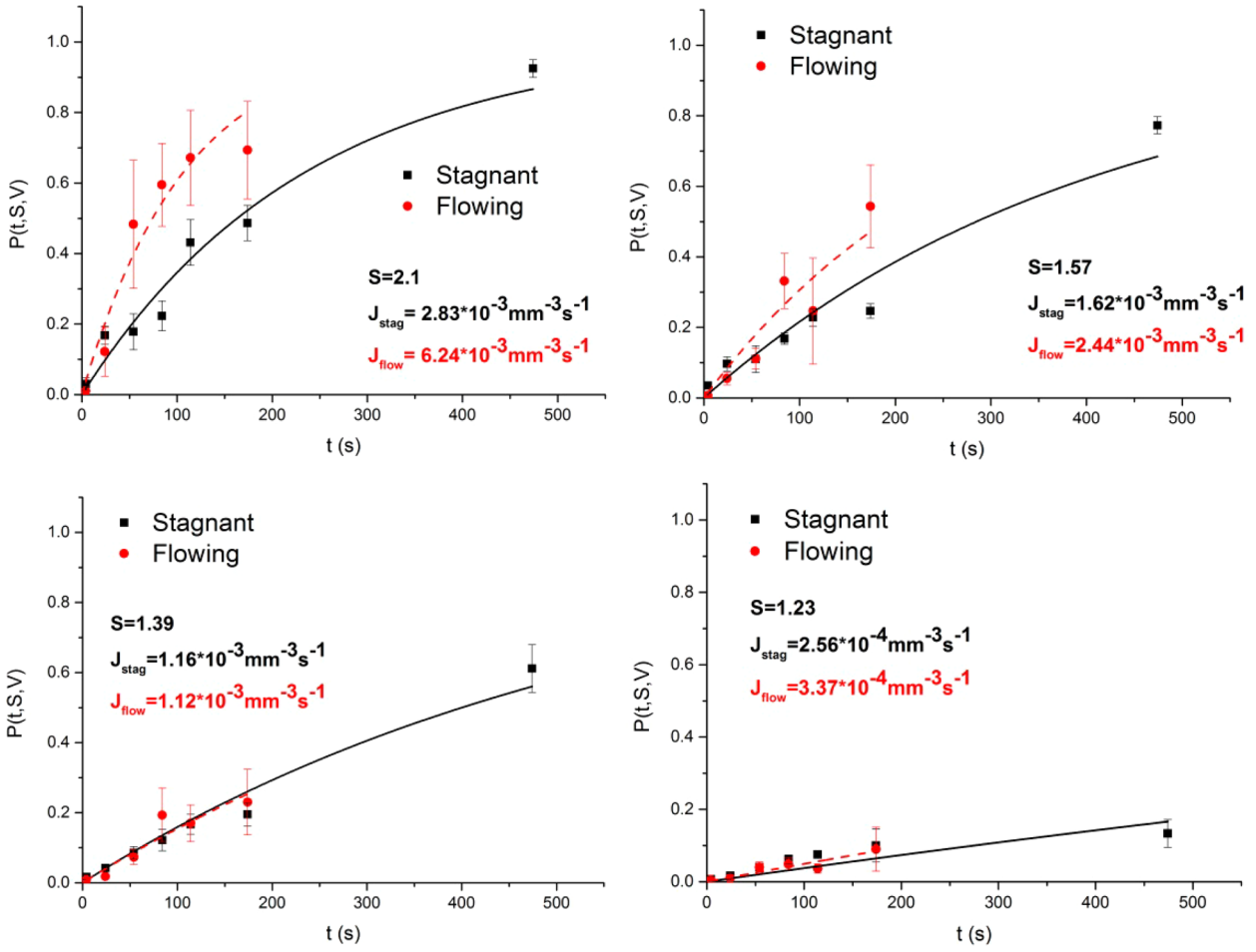

Figure 6. Adipic acid nucleation rate determined by fitting the experimental points of the cumulative distribution function at different residence times for various supersaturations with the theoretical cumulative distribution function.

Under both stagnant and flow experiments, we calculated the probability function $P_E(t;S,V)$ for different nucleation times (10, 30, 60, 90, 120, 180, and 480 s). Under flow conditions, these times were equal to the residence times of the fluid in the nucleation section; these were obtained by using capillary tubes of 0.167, 0.5, 1, 1.5, 2, and 3 m, respectively. To check the reproducibility of the results, we repeated each experiment three times, calculating mean values and standard deviations. Since the experimental procedure requires cooling the droplet arrays from the initial temperature T_1 to the nucleation temperature T_2, a time lag t^* was present for the achievement of the specific supersaturation $S(T_2)$. According to COMSOL simulations (refer to the Supporting Information), the fluid temperature reaches the constant value T_2 over a distance along the capillary axis corresponding to a residence time of $t^* = 6$ s, starting from the temperature T_1 for both stagnant and flow conditions. Supposing that no nucleation events take place during the achievement of the temperature T_2 (refer to the Supporting Information for details), we determined the nucleation rates by shifting the origin of the time axis by 6 s ($t' = t - t^*$). Hence, the rescaled residence times are $t' = 4$, 24, 54, 84, 114, 174, and 474 s, respectively.

The longest nucleation time investigated under stagnant conditions (480 s) was not considered in flow experiments due to the necessity to operate with a very long capillary tube (8 m), which results in pressure drops that are too high for the syringe pumps employed.

4. RESULTS AND DISCUSSION

4.1. Determination of Nucleation Rates. Figure 6 shows the cumulative distribution function for the four different supersaturation levels considered under stagnant and flow conditions. As expected, the higher the supersaturation, the larger the driving force and in turn the nucleation rate. The fitting functions reproduce very well the experimental points. This confirms that the stochastic process can be described by the Poisson model. At high supersaturation (S = 2.1, 1.57), nucleation rates are higher under flow conditions, while at lower supersaturation (S = 1.39, 1.23) the results are similar to those obtained in stagnant droplets. Moreover, the experimental error is larger at high supersaturation, especially under flow conditions.

4.2. Nucleation Parameters. The relation between the nucleation rate J and the supersaturation ratio S expressed as per eq 4 allows calculating the kinetic and thermodynamic parameters A and B, as described in section 2, by the best linear fit reported in Figure 7 for both stagnant and flow conditions.

After obtaining the values of A and B, we calculated the nucleation parameters given in eq 5. The results are reported in Tables 1 and 2. To calculate the crystal–liquid interfacial energy for homogeneous nucleation, we adopted Mersmann's equation,[27] setting the constant in the equation to 0.514, assuming a spherical nucleus.[20] Therefore, it is

$$\gamma = \frac{0.514KT}{v_0^{2/3}} \ln\left(\frac{1}{N_a v_0 C_e}\right) \quad (6)$$

where N_a is Avogadro's number (6.022×10^{23}) and C_e is the adipic acid equilibrium concentration[25] (68.43, 91.42, 103.73,

DOI: 10.1021/cg501836e
Cryst. Growth Des. 2015, 15, 1784−1791

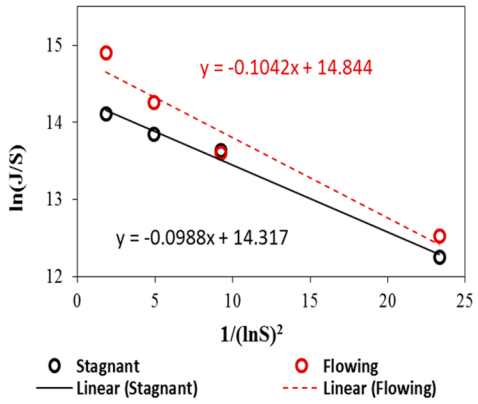

Figure 7. Fitting of nucleation rate equation $J(S) = AS \exp[-B/(\ln S)^2]$.

and 116.60 mol/m^3) calculated at the nucleation temperatures T_2 = 10 , 14, 16, and 18 °C, respectively.

If the data fitting of Figures 6 and 7 is performed without rescaling the time axis, the values of A increase by 5% and 7% for stagnant and flow regimes, respectively, while those of B increase by about 1% for both regimes. These differences are acceptable and are within the experimental error of the data fitting.

4.3. Discussion. Using eq 5, we may express the nucleation rate in terms of the nucleation parameters reported in Table 1, to obtain

$$J(S) = zf^*C_0 \exp\left(-\frac{W}{KT}\right) \tag{7}$$

For both regimes, the number of molecules in a critical nucleus n^* and (normalized) nucleation work barrier W/KT decrease with increasing supersaturation, since it is easier to form small stable nuclei at high supersaturation levels. This is quite intuitive, as the supersaturation is the driving force of the process.

The Zeldovich factor z, which accounts for the fraction of nuclei larger than the critical nucleus of n^* molecules that decay and disappear rather than growing to macroscopic size (probability for a stable nucleus to redissolve), is in the typical range of 0.01−1[18] for both stagnant and flow conditions. In this regard, we should notice that not all the nuclei that reach the critical size turn into stable crystals: the probability of the nuclei at the top of the activation energy barrier to grow into stable crystal is less than unity. The Zeldovich factor z corrects $J(S)$ by taking into account the loss of stable nuclei owing to their Brownian motion. These are "escaped nuclei" that do not contribute to nucleation and thus reduce the nucleation rate.[20]

In case of homogeneous nucleation (HON), experimental estimations of A are generally on the order of 10^{26}−10^{30} m^{-3} s^{-1}, whereas for heterogeneous nucleation (HEN) A can assume values that are several orders of magnitude lower.[11,18]

Table 2. Interfacial Energy Ratio for Heterogeneous/Homogeneous Nucleation (γ_{eff}/γ)

	γ_{eff} (mJ m^{-2})		γ (mJ m^{-2})		γ_{eff}/γ	
S	stag	flow	stag	flow	stag	flow
1.23	2.23	2.27	31.13	31.13	0.071	0.073
1.39	2.26	2.30	29.71	29.71	0.076	0.077
1.57	2.27	2.31	29.10	29.10	0.078	0.080
2.10	2.29	2.33	28.54	28.54	0.080	0.082

The A values that we measured in our experiments are A_{stag}= 1.65 × 10^6 m^{-3} s^{-1} and A_{flow} = 2.8 × 10^6 m^{-3} s^{-1}. This suggests that heterogeneous nucleation should be the dominant nucleation mechanism. Accordingly, the low values of the heterogeneous crystal−liquid interfacial energy γ_{eff} in comparison to the homogeneous crystal−liquid interfacial energy γ results in low values of γ_{eff}/γ for stagnant and flow conditions (see Table 2). This confirms the dominant HEN mechanism for both regimes. The 2 μm filters employed to pretreat the adipic acid solution ensure no impurity particles larger than 2 μm are present but do not eliminate all foreign particles.

As nucleation is easier to achieve under heterogeneous conditions in comparison to homogeneous, one may expect that $A_{HEN} > A_{HON}$. This, however, does not have to be, because the nucleation rate $J(S)$ strongly depends on the exponential term of eq 7 and therefore on the thermodynamic factor B that appears in it. $J(S)_{HEN}$ can be larger than $J(S)_{HON}$ even if $A_{HEN} < A_{HON}$ as long as B_{HON} is considerably larger than B_{HEN}. This is what happens in our case: the nucleation rates $J(S)_{HEN}$ are orders of magnitude higher than the corresponding homogeneous rates evaluated considering the theoretical value of B calculated from the equation

$$B = \frac{4}{27}\frac{c^3 v_0^2 \gamma^3}{(KT)^3} \tag{8}$$

where γ is given in eq 6. The values obtained are B_{HON} = 219, $B_{HEN,stag}$ = 0.0988, and $B_{HEN,flow}$ = 0.1042, which result in $J(S)_{HEN} \gg J(S)_{HON}$.

Narducci et al.[28] investigated the nucleation rate of adipic acid in a continuous cooling crystallization process conducted in a stirred crystallizer (MSMPR). This is a large, and accordingly deterministic, system; thus, to model the process, the authors used a population balance equation. To derive nucleation rates, they fitted the crystal size distribution in the stream, leaving the crystallizer obtained numerically with that measured experimentally. The shapes of the distributions reflect the effect not only of primary nucleation but also of secondary nucleation, breakage, and agglomeration. These mechanisms are difficult to consider separately when one adopts a deterministic approach, and so one ends up with a "global" nucleation rate, which combines primary and secondary nucleation. Conversely, the stochastic method adopted in this work allows considering only primary nucleation, as we

Table 1. Nucleation Parameters under Stagnant and Flow Conditions

	$J(S)$ (10^6 m^{-3} s^{-1})		A (10^6 m^{-3} s^{-1})		B		n^*		W/KT		z		f^*C_0 (10^7 m^{-3} s^{-1})	
S	stag	flow	stag	flow	stag	flow	stag	flow	stag	flow	stag	flow	stag	flow
1.23	0.256	0.337	1.65	2.8	0.0988	0.1042	22.27	23.49	2.31	2.43	0.022	0.022	9.14	15.91
1.39	1.16	1.12					5.53	5.84	0.91	0.96	0.056	0.055	4.08	7.10
1.57	1.62	2.44					2.15	2.27	0.48	0.51	0.105	0.103	2.45	4.28
2.10	2.83	6.24					0.48*	0.51*	0.18	0.19	0.285	0.278	1.21	2.11

DOI: 10.1021/cg501836e
Cryst. Growth Des. 2015, 15, 1784−1791

discussed in section 2. Thus, the higher values of nucleation rates (10^{11}–10^{12} m^{-3} s^{-1}) found by Narducci et al.[28] in comparison to our values are not surprising. Such a difference is most probably due to the large occurrence of secondary nucleation and breakage in the MSMPR crystallizer promoted by the shear created by the stirrer and the vigorous fluid mixing.

Our results indicate that the flow conditions do not have a significant effect on the thermodynamics of the nucleation process, increasing the B parameter only from 0.0988 to 0.1042 and consequently leading to very small differences in the other parameters such as n^*, W/KT, z, and γ_{eff}. This is reasonable, as these variables have a thermodynamic origin and are unrelated to flow. Moreover, as the calculated variation of B from stagnant to flow is about 5%, which is within the experimental error, we conclude that the internal droplet mixing does not affect the thermodynamic parameter B at all. We should note that the values of n^* obtained for $S = 2.1$, reported in Table 1 (followed by an asterisk), are lower than unity; this implies that stable nuclei are formed by less than one molecule. This result makes no physical sense and has to be discarded. The reason for this is that the classical nucleation theory applies solely to nuclei of large enough size (more than a few molecules). When the value of n^* approaches unity, one needs to resort to the atomistic model of nucleation to calculate the values of n^*.[20] In the latter, the critical nucleus size has a discrete character, not being a continuous function of the supersaturation ratio. Supersaturation ranges are present in which the size of the critical nucleus is invariant. In such a model, the number of molecules in the critical nucleus can vary only discretely and cannot be less than unity.

Different conclusions arise from the analysis of the A factor, which accounts for the kinetics of the nucleation process. While the flow conditions do not affect the thermodynamics of the process, a remarkable variation is observed for the A factor, which changes from 1.65×10^6 m^3 s^{-1} (stagnant conditions) to 2.8×10^6 m^3 s^{-1} (flow conditions). A difference of more than 30% cannot be related to experimental error and consequently can be only explained by a change in the kinetics of nucleation. Experiments show that $J(S)_{flow}$ is larger than $J(S)_{stag}$ and this gap arises from the pre-exponential term zf^*C_0 and in particular from the product f^*C_0, which accounts only for the kinetics of the process. In fact, as the Zeldovich factor remains constant in both regimes, the term f^*C_0 dominates in flow conditions, making $J(S)_{flow}$ exceed $J(S)_{stag}$. Therefore, we may hypothesize that the recirculation present within the droplets in flow conditions[24] increases $J(S)$ by enhancing the attachment frequency f^*. This increases because convection renders the flux of monomers toward the nucleus surface larger. This hypothesis is supported for example in the case of capillary liquid–liquid reactions by the enhancement of mass transfer coefficients registered at high slug flow velocities[29] or mechanical mixing.[30] The enhancement of mass transfer is interpreted in terms of internal circulation flow within the plugs, a conclusion corroborated by CFD calculations. The attachment frequency f^* has been determined theoretically for spherical nuclei and HON in *diffusion-controlled* processes with less concentrated solutions and *interface-controlled* processes with highly concentrated solutions.[20] The resulting formulas show a direct proportionality between f^* and the monomer diffusion coefficient D ($f^* \propto D$).[18] The theoretical determination of f^* when nucleation occurs on a substrate (HEN) is still a problem under investigation owing to the inhomogeneity of the concentration field around the foreign substrate, which complicates the calculation of the monomer flux. This makes it difficult to estimate f^* in our case, because under both flow and stagnant conditions the nucleation mainly occurs heterogeneously. We cannot even calculate f^* experimentally from the known product f^*C_0, since in heterogeneous nucleation we cannot estimate the concentration of nucleation sites C_0 in the system. This problem does not arise in HON, where one assumes that each molecule in the solution gives a nucleation site from which a nucleus can grow and possibly become stable (so that $C_0 = 1/v_0 \approx 10^{28}$–$10^{30}$ m^{-3}). This also explains why A is much higher in HON than in HEN, as the concentration C_0 tends to be considerably higher in the case of HON than in HEN.

We conclude that mixing tends to enhance the nucleation rate by increasing the mass transfer of monomers toward the surface of the forming nucleus. This is reflected by a rise in the attachment frequency f^*. The recirculation within the flowing droplets does not affect the thermodynamics of primary nucleation, as the enhancement of f^* is not accompanied by a drop in the nucleation work barrier represented by the B factor.

The recirculation patterns inside the droplets do not always cover the entire droplet volume: the patterns depend on the mixture velocity and capillary cross-section profile.[31,24] This fluid dynamic inhomogeneity within the droplet samples, due to the presence of stagnation and mixed areas, may explain the larger spread of values observed in flow experiments. Moreover, the small difference in $J(S)$ values at low supersaturation (S = 1.39, 1.23) between stagnant and flow conditions could be due to the fact that recirculation within the droplets may not play a significant role when the cluster concentration is relatively low.

The validity of the values of the nucleation rate parameters reported in the article is guaranteed only within the ranges of supersaturation ratio and operating conditions considered. We expect that they should also be valid outside these ranges, provided the nucleation mechanism remains the same. As was said, in our experiments we opted to work at low temperature because this allowed us to control the temperature better during the counting process. This was performed at a temperature (T_3) that is close to room temperature (T_{room}) and was in a part of the metastable zone where no nucleation takes place (refer to section 3.2).

5. CONCLUSIONS

Large stirred crystallizers are commonly employed to derive nucleation rates by fitting the crystal size distribution derived numerically with that measured experimentally. Unfortunately, due to the deterministic volumes adopted and the number of processes occurring during the mixing (e.g., secondary nucleation, agglomeration, etc.), it is difficult to obtain a valid expression for the primary nucleation rate. In this work, we developed a microdroplet-based system to measure the primary nucleation rate of adipic acid solutions by cooling crystallization in millichannels under two different fluid dynamic conditions. We derived crystal primary nucleation kinetics by probability distribution functions under stagnant (motionless droplet) and flow (moving droplet) conditions, determining nucleation rates, kinetic and thermodynamic parameters, and characteristic nuclei parameters using the mononuclear nucleation mechanism and the classical nucleation theory. The results indicate that the nucleation of the adipic acid solution occurs predominantly by a heterogeneous mechanism in both cases. The mixing patterns achieved inside the moving droplets

DOI: 10.1021/cg501836e
Cryst. Growth Des. 2015, 15, 1784–1791

accelerate the nucleation rates $J(S)$. This is due to the enhancement of the attachment frequency by the increase of the flux of monomers toward the nucleus surface by convection. The evaluation of the thermodynamic factor B for both regimes and related parameters demonstrate that flow conditions do not promote primary nucleation (they do not lower the nucleation energy barrier). The evaluation of the effective crystal−liquid interfacial energy γ_{eff} over the theoretical homogeneous crystal−liquid interfacial energy γ determined for both regimes demonstrates the dominance of heterogeneous nucleation over homogeneous nucleation in both circumstances.

■ ASSOCIATED CONTENT

Supporting Information

Text and figures showing that, as reported in section 3, in calculating the values of the function $P_E(t;S,V)$ the assumption that no nucleation occurs while the adipic acid solution is cooled from the temperature T_1 to the desired nucleation temperature T_2 is acceptable. This material is available free of charge via the Internet at http://pubs.acs.org.

■ AUTHOR INFORMATION

Corresponding Author

*E-mail for L.M.: l.mazzei@ucl.ac.uk.

Notes

The authors declare no competing financial interest.

■ ACKNOWLEDGMENTS

Support from the EPSRC and GSK is gratefully acknowledged. In particular, we thank Dr. Matthew Hannan and Dr. Olga Narducci from GSK for useful discussions.

■ DEDICATION

This paper is dedicated to Professor Alan G. Jones, who passed away on August 13, 2014.

■ REFERENCES

(1) Davey, R. J.; Schroeder, S. L. M.; ter Horst, J. H. *Angew. Chem., Int. Ed. Engl.* **2013**, *52*, 2166−2179.

(2) Revalor, E.; Hammadi, Z.; Astier, J. P.; Grossier, R.; Garcia, E.; Hoff, C.; Furuta, K.; Okustu, T.; Morin, R.; Veesler, S. *J. Cryst. Growth* **2010**, *312*, 939−946.

(3) Kulkarni, S. A.; Kadam, S. S.; Meekes, H.; Stankiewicz, A. I.; ter Horst, J. H. *Cryst. Growth Des.* **2013**, *13*, 2435−2440.

(4) Leng, J.; Salmon, J. B. *Lab Chip* **2009**, *9*, 24−34.

(5) Squires, T. M. *Rev. Mod. Phys.* 2005, *77*.

(6) Anna, S. L.; Mayer, H. C. *Phys. Fluids* **2006**, *18*, 121512.

(7) Xu, J. H.; Li, S. W.; Tan, J.; Wang, Y. J.; Luo, G. S. 2006, *52*, 3005−3010.

(8) Galkin, O.; Vekilov, P. G. *J. Phys. Chem. B* **1999**, *103*, 10965−10971.

(9) Dombrowski, R. D.; Litster, J. D.; Wagner, N. J.; He, Y. *Chem. Eng. Sci.* **2007**, *62*, 4802−4810.

(10) Keller, D. M.; Massey, R. E.; Hileman, O. E., Jr. *Can. J. Chem.* **1978**, *56*, 831−838.

(11) Laval, P.; Salmon, J. B.; Joanicot, M. *J. Cryst. Growth* **2007**, *303*, 622−628.

(12) Kadam, S. S.; Kulkarni, S. A.; Coloma Ribera, R.; Stankiewicz, A. I.; ter Horst, J. H.; Kramer, H. J. M. *Chem. Eng. Sci.* **2012**, *72*, 10−19.

(13) Teychené, S.; Biscans, B. *Chem. Eng. Sci.* **2012**, *77*, 242−248.

(14) Goh, L.; Chen, K.; Bhamidi, V.; He, G.; Kee, N. C. S.; Kenis, P. J. A.; Zukoski, C. F.; Braatz, R. D. *Cryst. Growth Des.* **2010**, *10*, 2515−2521.

(15) Poe, S. L.; Cummings, M. A.; Haaf, M. P.; McQuade, D. T. *Angew. Chem., Int. Ed. Engl.* **2006**, *45*, 1544−1548.

(16) Ramkrishna, D. *Population Balances-Theory and Applications to Particulate Systems in Engineering*; Academic Press, London, 2000.

(17) Jiang, S.; ter Horst, J. H. *Cryst. Growth Des.* **2011**, *11*, 256−261.

(18) Kashchiev, D.; van Rosmalen, G. M. *Cryst. Res. Technol.* **2003**, *38*, 555−574.

(19) Kashchiev, D.; Verdoes, D.; van Rosmalen, G. M. *J. Cryst. Growth* **1991**, *110*, 373−380.

(20) Kashchiev, D. *Nucleation: Basic Theory with Applications*; Butterworth-Heinemann: Oxford, U.K., 2000.

(21) Jiang, S. Ph.D. Thesis, Crystallization Kinetics in Polymorphic Organic Compounds; Delft University of Technology, Delft, The Netherlands, 2009.

(22) Ildefonso, M.; Revalor, E.; Punniam, P.; Salmon, J. B.; Candoni, N.; Veesler, S. *J. Cryst. Growth* **2012**, *342*, 9−12.

(23) Garstecki, P.; Fuerstman, M. J.; Stone, H. A.; Whitesides, G. M. *Lab Chip* **2006**, *6*, 437−446.

(24) Dore, V.; Tsaoulidis, D.; Angeli, P. *Chem. Eng. Sci.* **2012**, *80*, 334−341.

(25) Mullin, J. W. *Crystallization*; Butterworth-Heinemann: Oxford, U.K., 2001.

(26) Liu, H.; Vandu, C. O.; Krishna, R. *Ind. Eng. Chem. Res.* **2005**, *44*, 4884−4897.

(27) Mersmann, A. *Crystallization Technology Handbook*; Marcel Dekker: New York, 2001.

(28) Narducci, O. Ph.D. Thesis, Particle engineering via sonocrystallization: the aqueous adipic acid system; London College, London, 2012.

(29) Dummann, G.; Quittmann, U.; Gröschel, L.; Agar, D. W.; Wörz, O.; Morgenschweis, K. *Catal. Today* **2003**, *79−80*, 433−439.

(30) Mullin, J. W.; Raven, K. D. Influence of mechanical agitation on the nucleation of some aqueous salt solutions. *Nature* **1962**, *195*, 35−38.

(31) Bringer, M. R.; Gerdts, C. J.; Song, H.; Tice, J. D.; Ismagilov, R. F. *Philos. Trans. A: Math. Phys. Eng. Sci.* **2004**, *362*, 1087−1104.

DOI: 10.1021/cg501836e
Cryst. Growth Des. 2015, 15, 1784−1791